HAL open science

Paired 10 Be sampling of polished bedrock and erratic boulders to improve dating of glacial landforms: an example from the Western Alps

Charlotte Prud'Homme, Riccardo Vassallo, Christian Crouzet, Julien Carcaillet, Jean-louis Mugnier, Joaquin Cortés-aranda

To cite this version:

Charlotte Prud'Homme, Riccardo Vassallo, Christian Crouzet, Julien Carcaillet, Jean-louis Mugnier, et al.. Paired 10 Be sampling of polished bedrock and erratic boulders to improve dating of glacial landforms: an example from the Western Alps. Earth Surface Processes and Landforms, 2020, 45 (5), pp.1168 - 1180. 10.1002/esp.4790 . hal-03102683v2

HAL Id: hal-03102683

https://hal.science/hal-03102683v2

Submitted on 18 Jan 2021

HAL is a multi-disciplinary open access archive for the deposit and dissemination of scientific research documents, whether they are published or not. The documents may come from teaching and research institutions in France or abroad, or from public or private research centers.

L'archive ouverte pluridisciplinaire **HAL**, est destinée au dépôt et à la diffusion de documents scientifiques de niveau recherche, publiés ou non, émanant des établissements d'enseignement et de recherche français ou étrangers, des laboratoires publics ou privés.

Distributed under a Creative Commons Attribution - NonCommercial 4.0 International License

EARTH SURFACE PROCESSES AND LANDFORMS
Earth Surf. Process. Landforms **45**, 1168–1180 (2020)
© 2019 The Authors. Earth Surface Processes and Landforms published by John Wiley & Sons Ltd
Published online 27 February 2020 in Wiley Online Library
(wileyonlinelibrary.com) DOI: 10.1002/esp.4790

Paired ^{10}Be sampling of polished bedrock and erratic boulders to improve dating of glacial landforms: an example from the Western Alps

Charlotte Prud'homme,[1,2]* Riccardo Vassallo,[1] Christian Crouzet,[1] Julien Carcaillet,[1] Jean-Louis Mugnier[1] and Joaquin Cortés-Aranda[1,3]
[1] Université Grenoble Alpes, Université de Savoie-Mont-Blanc, CNRS, IRD, ISTerre, Grenoble, France
[2] Research Group for Terrestrial Palaeoclimates, Max Planck Institute for Chemistry, Mainz, Germany
[3] Departamento Ciencias de la Tierra, Universidad de Concepcion, Concepcion, Chile

Received 19 February 2019; Revised 4 December 2019; Accepted 5 December 2019

*Correspondence to: Charlotte Prud'homme, Research Group for Terrestrial Palaeoclimates, Max Planck Institute for Chemistry, Hahn Meitner-Weg 1, 55128 Mainz, Germany. E-mail: c.prudhomme@mpic.de
This is an open access article under the terms of the Creative Commons Attribution-NonCommercial License, which permits use, distribution and reproduction in any medium, provided the original work is properly cited and is not used for commercial purposes.

ESPL
Earth Surface Processes and Landforms

ABSTRACT: Cosmogenic nuclide dating of glacial landforms may lead to ambiguous results for ice retreat histories. The persistence of significant cosmogenic concentrations inherited from previous exposure may increase the apparent exposure ages for polished bedrocks affected by limited erosion under ice and for erratic boulders transported by glaciers and previously exposed in high-altitude rock walls. In contrast, transient burying by moraines, sediments and snow decreases the apparent exposure age. We propose a new sampling strategy, applied to four sites distributed in the Arc and Arve valleys in the Western Alps, to better constrain the factors that can bias exposure ages associated with glacial processes. We used the terrestrial cosmogenic nuclide ^{10}Be (TCN) to estimate the exposure time from paired sampling of depth profiles in polished bedrock and on overlying erratic boulders. For a given sampling site, the exposure ages for both the polished bedrock and boulder are expected to be the same. However, in six cases out of seven, boulders had significantly higher ^{10}Be surface concentrations than those of the associated polished surfaces. In present and past glacial processes, the ^{10}Be distribution with depth for boulders and bedrocks implies the presence of an inheritance concentration of ^{10}Be. Our study suggests that ^{10}Be concentrations in erratic boulders and in polished bedrocks provide maximum and minimum exposure ages of the glacial retreat, respectively. © 2019 The Authors. Earth Surface Processes and Landforms published by John Wiley & Sons Ltd

KEYWORDS: glacial landforms; polished bedrocks; erratic boulders; ^{10}Be dating

Introduction

The dynamics of glacial erosion/transport and their impact on landscape on a Quaternary timescale are difficult to quantify (Menzies, 2018, and references therein). In contrast to a fluvial system, the long advance and retreat ice periods of glaciers (10^2–10^3 years) combined with the difficulty of observing processes at the ice/bedrock contact make it challenging to understand the ongoing processes involved (Ganti et al., 2016). The actions of a glacier are sensitive to various parameters: the thermal state at the ice base, the ice-sliding velocity, the thickness of the transported till and the bedrock topography (Herman et al., 2015). These parameters vary spatially under a glacier and are difficult to estimate for earlier times. Glaciers are often thought of as raw erosion agents that easily bevel all types of rocks while moving. However, consolidated Quaternary deposits can be poorly preserved on one side of a valley, while resistant bedrock can be carved simultaneously by the same glacier on the other side. Several examples are present in the Alps, such as the Baumkirchen paleolake sequence in the Austrian Inn valley (Barrett et al., 2017) and in the French Isère valley north of Grenoble (Fourneaux, 1976; Nicoud et al., 2002). Furthermore, significant bedrock erosion may occur at one glacial stage, while no erosion is observed at the next glacial stage. Few constraints on the complexity of the pre-depositional history of the glacial sediment transport and their residence time within the catchment are known. Hillslope denudation rates, for the same lithology, may vary by one order of magnitude in very small areas (a few hundred square metres) (Böhlert et al., 2008; Godon et al., 2013). From their source to the final deposit, sediments may undergo supraglacial, subglacial and periglacial transport with extremely different dynamics and rates. All of these aspects have strong implications for the dating of glacial landforms by terrestrial cosmogenic nuclides (TCN).

TCN is one of most used methods that can date the formation of glacial landforms. Other geochronometers such as radiocarbon (^{14}C) in organic matter or optical stimulated luminescence

(OSL) can be used; however, these methods have several limitations. In glacial or paraglacial environments, the scarcity of organic matter for ^{14}C dating makes this technique difficult to apply. Additionally, the age of the organic remains might not correspond exactly to the age of glacial retreat, as it can be older or younger following the sedimentation context. The main problem with OSL for buried sediments is the unbleaching relative to the glacial transport dynamics (King et al., 2014).

Dating of glacial morphologies by TCN (e.g. ^{10}Be, ^{26}Al, ^{21}Ne and ^{14}C) is based on the principle that cosmic rays begin to produce these elements in the rock surface after the ice has retreated. During the previous glacial stage, ice attenuates TCN production in the rock surface and can also erode the top several metres of rock containing inherited TCN, effectively resetting surface exposure clock. 10 m thick ice is sufficient to strongly attenuate ^{10}Be production induced by neutrons (Guillon et al., 2015).

The main assumption for dating polished surfaces is that, before being exposed to cosmic rays, the bedrock has to be previously eroded to a sufficient depth by glacial activity to completely reset the TCN chronometer. A local denudation of 2–3 m, the depth at which the attenuation of cosmic rays in rocks prevents the formation of significant cosmogenic ^{10}Be at a timescale of thousands of years, is the minimum needed for the applicability of this hypothesis. The main assumption for erratic boulders is that the accumulation of ^{10}Be in the rocks on the hillslopes and during sediment transport is negligible compared to the concentrations acquired at their final locations. When these assumptions are correct, the post-glacial apparent exposure age of the dated rock (polished surface or erratic boulder) is calculated using the nuclide concentration at the surface. However, the reality is often more complex, and several parameters that pre-date or post-date the glacial retreat can bias this age. The main factors influencing TCN ages are: (1) multiple exposures of the surface due to low denudation rates during glacial stages (affecting both polished surfaces and erratic boulders), or due to transport dynamics (erratic boulders); (2) the post-glacial denudation/degradation rates of the dated rocks; and (3) the temporary burial of the surface (snow, soil and/or sediments (e.g. till)).

Several examples of this complexity have been observed for past glacial valleys in the Alps and in the Pyrenees (Fabel et al., 2002; Delmas et al., 2008; Chenet et al., 2016; Protin et al., 2019). Erratic boulders with exposure cosmogenic ages from the last glacial period lie on older polished surfaces (Delmas et al., 2011). Conversely, erratic boulders yielding apparent exposure ages older than the last glacial period are abandoned on polished surfaces of the Last Glacial Maximum (Delmas et al., 2011). At the local scale of an outcrop, significant differences in exposure ages can exist on the same polished surface over a few metres (Delmas, 2009). A single moraine may consist of boulders with cosmogenic concentrations varying over a range of one order of magnitude (Graf et al., 2015). Hence the conversion of ^{10}Be concentration to exposure age is not always straightforward or unique and indicates significant discrepancies in glacial histories. Therefore, it is important to develop a methodological strategy that is able to discriminate the different contributions to the final concentration in a glacial landform to face this problem. Our paper presents a new sampling strategy based on the depth profile ^{10}Be concentration of polished surfaces and associated erratic boulders to determine the relationships between these glacial landforms and their apparent exposure ages. We have applied this method to four sites located in the Arve and Arc valleys in the Western French Alps (Figure 1).

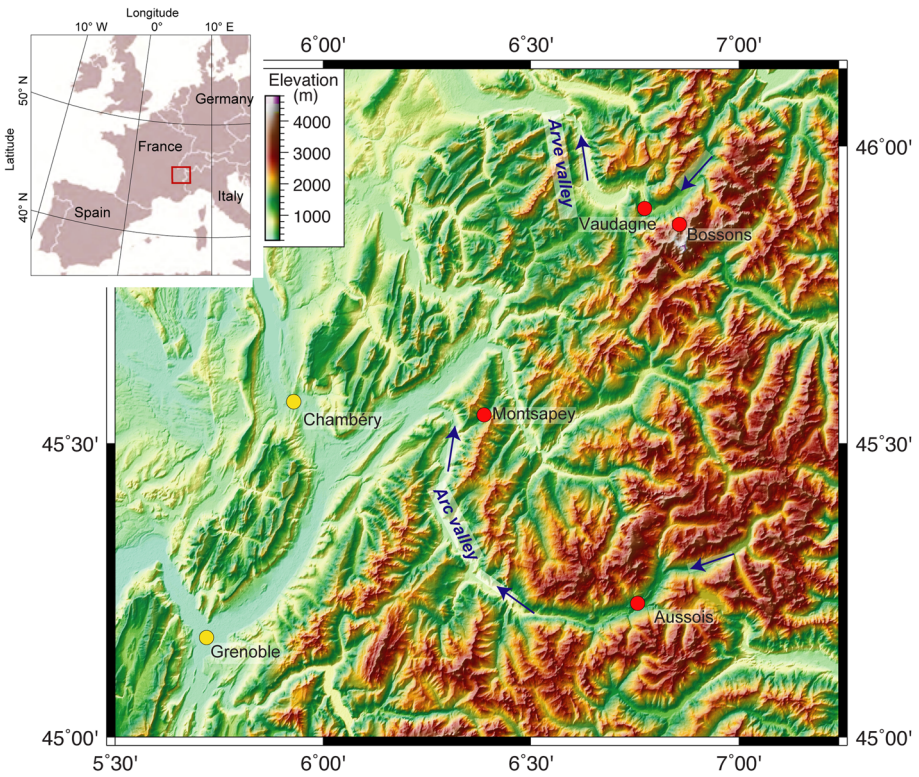

Figure 1. Elevation map of the French Alps. The red circles represented the locations of the four different sites located in the Arve (Vaudagne and Les Bossons) and Arc (Montsapey and Aussois) valleys. The yellow circles indicate the locations of Grenoble and Chambery. The blue arrows indicate the stream flows in the Arc and Arve valleys. [Colour figure can be viewed at wileyonlinelibrary.com]

© 2019 The Authors. Earth Surface Processes and Landforms published by John Wiley & Sons Ltd

Methods and Site Choice

Sites and sampling strategy

The four study sites, located in two glacial valleys of the Western Alps, were selected based on three fundamental conditions: (1) the presence of quartz-rich erratic boulders overlying well-preserved quartz-rich polished bedrock, as the mineral target for ^{10}Be is quartz; (2) evidence of good preservation of landforms from denudation and degradation since the glacial retreat; and (3) the absence of till material excluding a possible important burial thickness in the past. The sampling strategy is based on a paired sampling of polished bedrock and overlying erratic boulders at the same site, assuming that the two landforms have the same post-glacial retreat exposure age (Figure 2). Depth profiles on polished bedrock and large erratic boulders were collected, in addition to surface samples, to obtain a better constraint on the pre-exposure component processes.

On the Mont Blanc hillslopes and in the underlying Arve valley, we selected two sites that were close to the glacier source (Figure 1): the first was at the front of the present Bossons Glacier (BOSS12, 1700 m a.s.l.; Figure 3) and the second was at Vaudagne village, ~10 km downstream (VAU12, 1025 m a.s.l.; Figures 4 and 5), where the glacier has retreated since the last glacial period. The Arve valley was shaped by successive glaciers during the cold episodes of the Pleistocene. Glaciers are still present at high altitude in the Mont Blanc Massif. The mapping and dating of moraines in this area indicate that deglaciation took place in several steps during the Late Glacial (Coutterand and Nicoud, 2005; Protin et al., 2019).

In the Arc valley, two sampling sites were located several kilometres downstream from the glacial source: Montsapey (MSAP12) at 1005 m a.s.l. and Aussois (AUSS12) at 1470 m a.s.l., which are located 65 km apart. In Aussois, the dolomite bedrock was very well preserved, with visible striations and Neolithic rupestrian engraving (Nehl, 1981; Thirault, 2008), suggesting an absence of post-glacial erosion.

For each sample, the surrounding topographic shielding was calculated using a topographic shielding calculator (http://stoneage.ice-d.org). The geomorphic scaling factors were estimated using a clinometer and compass (Dunne et al., 1999). The majority of the boulders were sampled on their tops with a thickness of 2 cm, with no self-shielding. The boulder at the Bossons site was sampled on different faces, and relative strikes and dips were measured to estimate self-shielding. Bottom samples from large boulders (>2 m diameter) are considered to accumulate negligible ^{10}Be in their present positions. All surface samples were collected using a hammer and chisel. The bedrock and erratic boulder depth profiles (down to 3 m) at Vaudagne and Montsapey were sampled by the SAMSCIE company, who used a drill machine (model DK52, brand WEKA) equipped with a mining drill with diameters of 65 mm and 90 mm (Figure 6). After opening the cores at ISTerre Chambery, we cut four to five samples of 2–5 cm thick for each profile (Table I). At Aussois, a vertical profile in the polished bedrock was accessible in an abandoned quarry, and samples at various depths were collected using a hammer and chisel (Figure 7).

Analytical procedure

Sample preparation was carried out using the ISTerre GeoThermoChronology platform (Chambéry and Grenoble, France). Samples were crushed and sieved (250–500 μm). The quartz isolation was performed first by physical separation using a Frantz magnetic separator and then by chemical extraction doing repeated etching with a mixture of one-third HCl and two-thirds H_2SiF_6. Potential pollution by atmospheric ^{10}Be was removed from the separated quartz by sequential etching (3 × 10%) of samples three times with concentrated HF. The decontaminated quartz was spiked with 300 mg of a ^{9}Be standard solution (Scharlau beryllium standard solution, 1000 mg L^{-1} beryllium oxide form). Following the protocol established by Brown et al. (1991) and modified by Merchel and Herpers (1999), samples were then completely dissolved

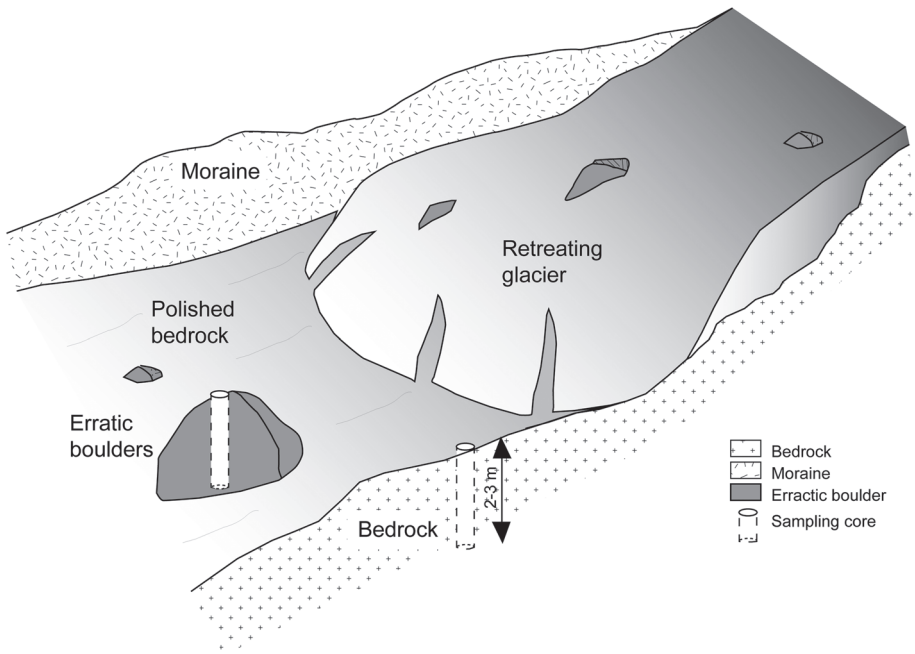

Figure 2. Sampling strategy for depth profile in erratic boulders and polished bedrocks. Erratic boulders and bedrock were sampled using a drill machine (model DK52, brand WEKA) equipped with a mining drill with diameters of 65 mm and 90 mm. The cores of 3 m are illustrated by white cylinders in the figure. Surface samples were also collected.

© 2019 The Authors. Earth Surface Processes and Landforms published by John Wiley & Sons Ltd

in HF. Afterwards, they were separated and purified by chromatography on anionic and cationic exchange resins (Dowex 1X8 and Dowex 50WX8), and precipitation stages were performed to isolate the beryllium. Finally, samples were heated to 900°C to oxidize the beryllium (BeO). The BeO samples were then mixed with niobium powder for target preparation before processing by accelerator mass spectrometry at the ASTER AMS facility (Aix en Provence, France; Arnold et al., 2010). The results of the BeO blank values are listed in the note to Table I. Measurements of $^{10}Be/^{9}Be$ ratios were normalized against NIST Standard Reference Material 4325 using an assigned $^{10}Be/^{9}Be$ ratio of 2.79×10^{-11} (Nishiizumi et al., 2007). Absolute uncertainties include the conservative errors of ~0.5% (Arnold et al., 2010), analytical errors (AMS counting statistics and AMS external errors) and propagation of the chemical blank measurements.

Age calculation

We used two methods to calculate the exposure ages from ^{10}Be concentrations of our samples: (1) CRONUS-Earth online calculator (http://hess.ess.washington.edu) to estimate exposure age of surface samples; and (2) the Monte Carlo approach developed by Hidy et al. (2010) to modelling exposure ages from depth profiles (^{10}Be profile simulator version 1.2, running on MATLAB™ 2015b).

Surface ^{10}Be exposure ages were calculated using the CRONUS-Earth online calculator method with the time-dependent scaling scheme of Lal (1991)/Stone (2000) (Lal, 1991; Stone, 2000; Balco et al., 2008). To compare our results with other studies, we used the Arctic ^{10}Be production rate of 3.930 ± 0.150 atoms g^{-1} yr^{-1} (Young et al., 2013). This parameter was corrected for sample thickness, sample density ($2.7\ g\ cm^{-3}$), sample elevation, latitude and the topographic shielding correction (Table I). Since there is no information concerning snow cover over several thousand years at the different sites, we chose to consider no corrections for snow burial. Moreover, the impact of snow cover on the relative ages at a local scale should be minimal. The present-day snow thickness can be quantified at ~1 m for 6 months, which is extrapolated to the entire exposure period, resulting in an absolute age underestimation on the order of 10%.

The exposure ages from the ^{10}Be concentration depth profiles of Vaudagne, Montsapey and Aussois were calculated using a ^{10}Be profile simulator developed by Hidy et al. (2010). This model, based on a Monte Carlo approach, estimates the most probable values for exposure age, erosion rate and inherited nuclide concentration while providing a rigorous treatment of their uncertainties. The model simulations were run using specific parameters for each site. The site-specific scaling of the neutron-induced spallogenic surface production rates (Stone, 2000) and the muonic component of TCN production (Balco et al., 2008; Hidy et al., 2010) were included in the site-specific parameters. The length attenuation for neutrons was fixed at $160\ g\ cm^{-2}$ (Balco et al., 2008; Hidy et al., 2010). In our modelling, we fixed null denudation rates for both boulders and polished surfaces, and we enabled the inheritance nuclide concentration to vary from 0 to the lowest ^{10}Be concentration of a profile (between 2 and 3 m deep). The dataset parameters for each site and the exposure ages are regrouped in Table I and the parameter setups used by the Monte Carlo simulations are summarized in Table II.

Results

In this study, 35 samples collected from four sites are presented: 13 samples from seven erratic boulders and 22 samples from four polished bedrocks. The details of samples and ^{10}Be concentrations are reported in Table I and Figures 3, 4 and 5 for the Arve valley and in Figures 6 and 7 for the Arc valley. Apparent exposure ages were deduced from the mean, minimum and maximum values using the Monte Carlo approach of Hidy et al. (2010) (Table II).

Mont Blanc hillslope and Arve valley

The first site is located at the frontal zone of the Bossons glacier at 1700 m a.s.l. The ice retreated just a few years ago and the 20 m thick frontal part of the glacier is still present a few metres to the side. Three samples were collected on different faces of a 3 m diameter granite erratic boulder (BOSS12_B1). This boulder fell on the polished bedrock after being released from the glacial ice in 2012 (Figure 3). Its abandonment age is a few years old. Two fragments (BOSS12_B1_01 and BOSS12_B1_02), having the same ^{10}Be concentrations (1.20 ± 0.54 and $1.24 \pm 0.21 \times 10^4$ atoms g^{-1}) but with different shielding correction factors, yielded similar apparent exposure ages of 0.83 ± 0.37 ka and 1.08 ± 0.18 ka (Table I). The third face (BOSS12_B1_03), which is characterized by a darker varnish, has a higher ^{10}Be concentration ($2.57 \pm 0.44 \times 10^4$ atoms g^{-1}) and an older apparent exposure age of 3.66 ± 0.64 ka. Additionally, two samples were collected from the polished bedrock surface (CRO12_P1). CRO12_P1_02 has a ^{10}Be concentration of $1.31 \pm 0.58 \times 10^4$ atoms g^{-1}, corresponding to an apparent exposure age of 0.91 ± 0.42 ka, and CRO12_P1_04 has a lower ^{10}Be concentration ($0.83 \pm 0.42 \times 10^4$ atoms g^{-1}), which corresponds to an apparent exposure age of 0.58 ± 0.29 ka.

The second sampling site in the Arve valley is Vaudagne, located 10 km downstream from the Bossons Glacier at 1030 m a.s.l. Paired samplings of polished bedrock and erratic boulder were performed at two sites in Vaudagne, located 1 km apart.

Site 1 (VAU12-P1 and B1) is characterized by a 2 m diameter granite boulder lying on polished schist bedrock. Five samples from various depths were collected from the bedrock drill core (0, 30, 66, 107 and 305 cm). The ^{10}Be concentrations in the depth profile decrease exponentially from $9.60 \pm 0.77 \times 10^4$ atoms g^{-1} at the surface to $0.57 \pm 0.15 \times 10^4$ atoms g^{-1} at 305 ± 2.5 cm (Figure 4). The CRONUS-Earth online calculator gives a surface exposure age of 10.08 ± 0.90 ka, based on one surface sample. For comparison, the ^{10}Be profile simulator (Hidy et al., 2010) generates a most probable exposure age of 10.10 ± 1.90 ka, associated with an inheritance of $0.43 \pm 0.39 \times 10^4$ atoms g^{-1} (Tables I and II). Two samples were collected from the boulder: one at the top and one at the bottom. The ^{10}Be concentrations of these two samples are $21.37 \pm 1.61 \times 10^4$ atoms g^{-1} and $11.45 \pm 1.79 \times 10^4$ atoms g^{-1}, for the top and bottom. Based on only the top sample, the CRONUS-Earth online calculator calculates an exposure age of 22.33 ± 1.89 ka. By contrast, assuming a pre-exposure history leading to homogeneous inheritance before abandonment, the most probable exposure age of the boulder using the Hidy simulation is 11.20 ± 3.90 ka, associated with an inheritance of $11.16 \pm 6.49 \times 10^4$ atoms g^{-1} (Table II).

Site 2 (VAU12-P2 and B2) is characterized by a granite boulder of 8–9 m^3 lying on polished granite bedrock. Six samples were collected from the bedrock drill core at 0 ± 2, 30 ± 2.5, 135 ± 2.5, 235 ± 2.5, 260 ± 2.5 and 285 ± 2.5 cm depth, and three samples were collected from the erratic boulder at 0 ± 2, 92 ± 2.5 and

© 2019 The Authors. Earth Surface Processes and Landforms published by John Wiley & Sons Ltd

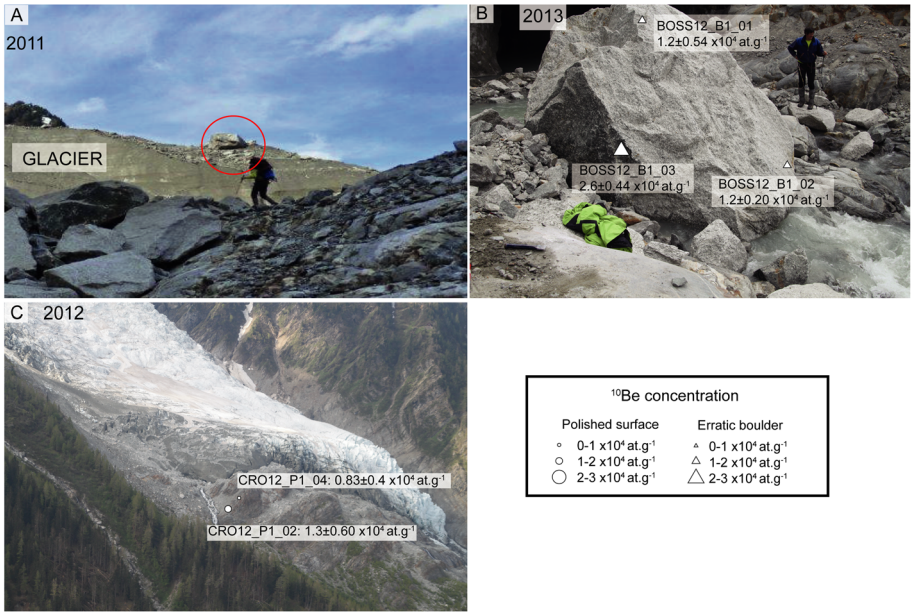

Figure 3. Les Bossons site: sample locations and ^{10}Be concentrations in erratic boulder (BOSS12_B1_01, BOSS12_B1_02 and BOSS12_B1_03) and in polished bedrock (CRO12_P1_02 and CRO12_P1_04). (A) Position of the erratic boulder in 2011 on the Bossons Glacier. (B) Same erratic boulder sampled in 2013 is no longer on the glacier but is on the bedrock. (C) Position of the glacier terminus of the Bossons in 2012 and positions of the two samples of polished bedrock. The circle and triangle represent the ^{10}Be concentrations in the polished bedrock and the erratic boulder, respectively. The size of these symbols is dependent on the ^{10}Be concentration. [Colour figure can be viewed at wileyonlinelibrary.com]

180 ± 2.5 cm depth. The ^{10}Be concentrations in the bedrock profile decrease exponentially from 15.55 ± 1.33 × 10^4 atoms g^{-1} (at the surface) to 2.19 ± 0.57 × 10^4 atoms g^{-1} (at 285 cm depth) and the ^{10}Be concentrations of the boulder range from 12.86 ± 1.37 × 10^4 atoms g^{-1} at the surface to 3.43 ± 0.64 × 10^4 atoms g^{-1} at 180 cm depth. The exposure ages for the polished bedrock and the boulder, based only on the surface samples (with CRONUS-Earth online calculator), are 16.41 ± 1.55 ka and 13.68 ± 1.55 ka, respectively. The ^{10}Be depth profile simulation for the bedrock yields a most probable exposure age of 15.70 ± 3.80 ka with an inheritance of 1.18 ± 0.87 × 10^4 atoms g^{-1}. Additionally, the most probable exposure age for the boulder, considering the three samples over depth, is 11.00 ± 3.10 ka with a homogeneous inheritance of 3.17 ± 1.89 × 10^4 atoms g^{-1} (Table II).

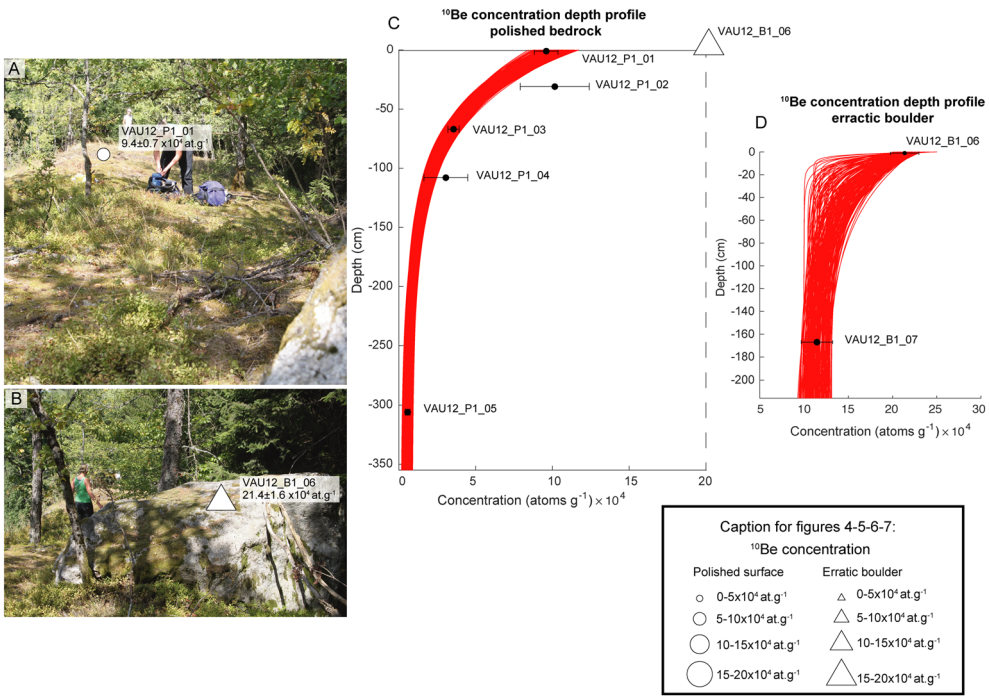

Figure 4. Vaudagne Site 1: sample locations and ^{10}Be concentrations in the erratic boulder (VAU12_B1_06 and VAU12_B1_07) and in the polished bedrock (VAU12_P1). (A) Polished bedrock (circles) and location of the core sampling. (B) Sampled erratic boulder (triangle) lying on the polished bedrock. The circles and triangles illustrate the sampling positions, and their sizes are dependent on the ^{10}Be concentrations of the samples. Results from the Monte Carlo concentration–depth profile simulation of (C) polished bedrock and (D) boulder; 2σ profile solution spaces (red line), measured ^{10}Be concentration samples with associated uncertainties (filled black circles and error bars). The input and output parameters of the concentration–depth profile simulation are reported in Table II. [Colour figure can be viewed at wileyonlinelibrary.com]

© 2019 The Authors. Earth Surface Processes and Landforms published by John Wiley & Sons Ltd

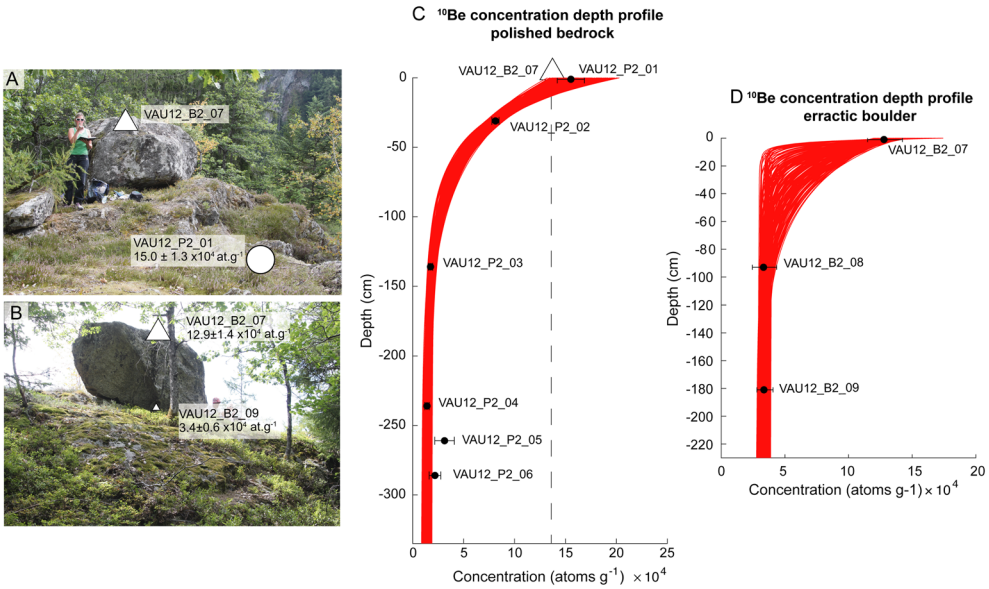

Figure 5. Vaudagne Site 2: sample locations and ^{10}Be concentrations in erratic boulder (VAU12_B2_7 and VAU12_B2_09) and in polished surface (VAU12_P2). (A) Polished bedrock with location of the core sampling and erratic boulder. (B) Sample locations of the erratic boulder. The circles and triangles illustrate the sampling positions, and their sizes are dependent on the ^{10}Be concentrations of the samples. Results from the Monte Carlo concentration–depth profile simulation of (C) polished bedrock and (D) boulder; 2σ profile solution spaces (red line), measured ^{10}Be concentration samples with associated uncertainties (filled black circles and error bars). The input and output parameters of the concentration–depth profile simulation are reported in Table II. [Colour figure can be viewed at wileyonlinelibrary.com]

Arc valley

At Montsapey, one boulder of 1 m diameter was sampled on its surface and five samples were collected from a drilled bedrock core at 0 ± 2, 31 ± 2.5, 52.5 ± 2.5, 91 ± 2.5 and 283 ± 2.5 cm depth. The granite erratic boulder has a surface ^{10}Be concentration of 14.24 ± 1.71 × 10^4 atoms g^{-1}. The ^{10}Be concentrations of the polished schist bedrock decreased exponentially from

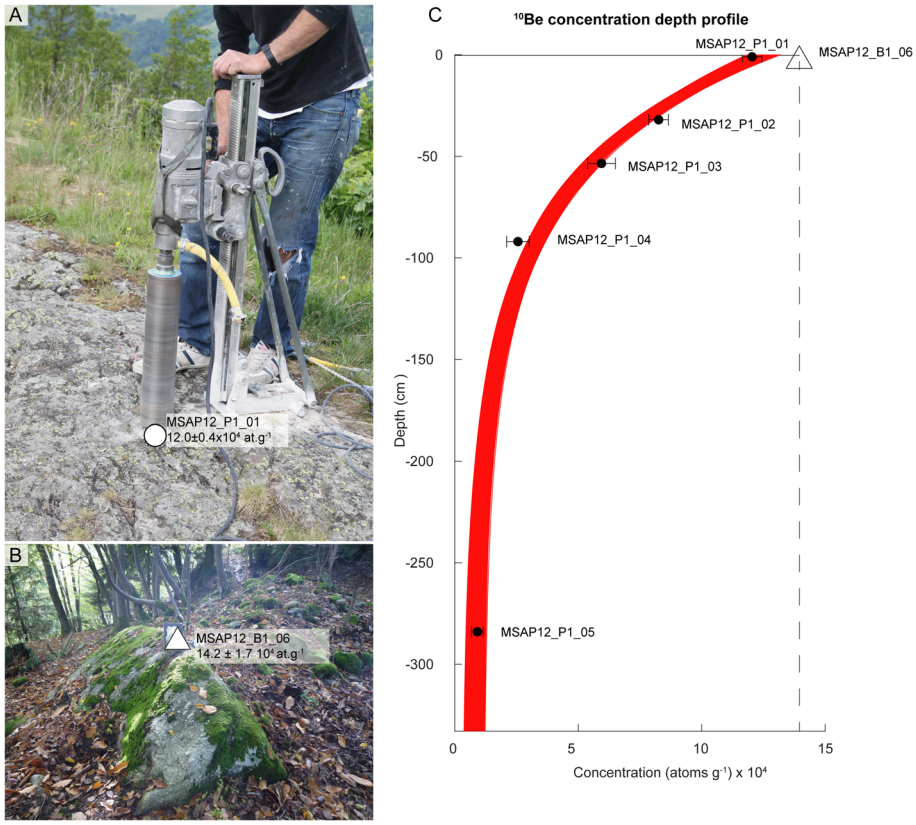

Figure 6. Montsapey site: sample locations and ^{10}Be concentrations in erratic boulder (MSAP12_B1_06) and polished surface (MSAP12_P1). (A) Sampling of the polished bedrock using a drilling machine (model DK52, brand WEKA), equipped with a mining drill with a diameter of 90 mm. (B) Erratic boulder and the sample position. The circles and triangles illustrate the sampling positions, and their sizes are dependent on the ^{10}Be concentrations of the samples. (C) Results from the Monte Carlo concentration–depth profile simulation of the polished bedrock; 2σ profile solution spaces (red line), measured ^{10}Be concentration samples with associated uncertainties (filled black circles and error bars). For comparison, we report the surface ^{10}Be concentration (dashed line) in the erratic boulder (white triangle). The input and output parameters of the concentration–depth profile simulation are reported in Table II. [Colour figure can be viewed at wileyonlinelibrary.com]

© 2019 The Authors. Earth Surface Processes and Landforms published by John Wiley & Sons Ltd

Table I. Sample details, ^{10}Be concentrations and calculated exposure ages from CRONUS and from Monte-Carlo concentration-depth profile simulations (^{10}Be profile simulator 1.2, cf. Hidy et al., 2010). NC are not communicated values. The samples are corrected from five different BeO blank values: * 1.022 x10^{-15}at.g^{-1}, **4.932x10–16 at.g^{-1}, ***7.908 x10–16 at.g^{-1}, **** 4.560x10^{-15} at.g^{-1} and ***** 6.920x10^{-16} at.g^{-1}. AMS analysis were performed at the French AMS facility ASTER. ^{10}Be concentration were calibrated against the NIST standard reference 4325 using an assigned ^{10}Be/^{9}Be ratio of 2.79±0.03x10^{-11} (Nishiizumi et al., 2007). A standard atmosphere and a rock density of 2.7 g.cm^{-3} were used. Erosion was not considered. For surface samples, the sample thickness is two cm below the surface. For deeper samples, "depth below bedrock" is the central point and the sample thickness is divided above and below the centre point. The surface ^{10}Be age exposures are calculated using the CRONUS-Earth online calculator (http://hess.ess.washington.edu) using the time-dependent scaling scheme of Lal (1991)/Stone (2000) (Balco et al., 2008; Lal, 1991; Stone, 2000) and with an Arctic ^{10}Be production rate of 3.930±0.150 atoms.g^{-1}.y^{-1} (Young et al., 2013). For the Monte-Carlo profile simulations, we selected the results from the mean, minimum and maximum values (table 2)

Site name	Sample name	Sample type	Lithology	Latitude (°)	Longitude (°)	Elevation (m)	Depth below bedrock (cm)	Sample thickness (cm)	Shielding correction	Production rate (at.g.yr^{-1})
Les Bossons	BOSS12_B1_01	Erratic Boulder	Granite	45.89132	6.85928	1700	0	2	0.910	14.29
	BOSS12_B1_02	Erratic Boulder	Granite	45.89132	6.85928	1700	0	2	0.800	14.29
	BOSS12_B1_03	Erratic Boulder	Granite	45.89132	6.85928	1700	0	2	0.450	14.29
	CRO12_P1_02	Polished bedrock	Granite	45.89141	6.85918	1762	0	2	0.910	14.29
	CRO12_P1_04	Polished bedrock	Granite	45.89141	6.85918	1762	0	2	0.910	14.29
Vaudagne Site 1	VAU12_P1_01	Polished bedrocks 1	Schist	45.90929	6.76412	1037	0	2	0.983	9.21
	VAU12_P1_02	Polished bedrock 1	Schist	45.90929	6.76412	1037	30	5	0.983	9.21
	VAU12_P1_03	Polished bedrock 1	Schist	45.90929	6.76412	1037	66	5	0.983	9.21
	VAU12_P1_04	Polished bedrock 1	Schist	45.90929	6.76412	1037	107	5	0.983	9.21
	VAU12_P1_05	Polished bedrock 1	Schist	45.90929	6.76412	1037	305	5	0.983	9.21
	VAU12_B1_06	Erratic Boulder 1	Granite	45.90929	6.76412	1037	0	2	0.983	9.21
	VAU12_B1_07	Erratic Boulder 1	Granite	45.90929	6.76412	1037	166	2	0.983	3.21
Vaudagne Site 2	VAU12_P2_01	Polished bedrock 2	Granite	45.90798	6.77030	1025	0	2	0.983	9.21
	VAU12_P2_02	Polished bedrock 2	Granite	45.90798	6.77030	1025	30	5	0.983	9.21
	VAU12_P2_03	Polished bedrock 2	Granite	45.90798	6.77030	1025	135	5	0.983	9.21
	VAU12_P2_04	Polished bedrock 2	Granite	45.90798	6.77030	1025	235	5	0.983	9.21
	VAU12_P2_05	Polished bedrock 2	Granite	45.90798	6.77030	1025	260	5	0.983	9.21
	VAU12_P2_06	Polished bedrock 2	Granite	45.90798	6.77030	1025	285	5	0.983	9.21
	VAU12_B2_07	Erratic Boulder 2	Granite	45.90798	6.77030	1025	0	2	0.983	9.21
	VAU12_B2_08	Erratic Boulder 2	Granite	45.90798	6.77030	1025	92	5	0.983	4.82
	VAU12_B2_09	Erratic Boulder 2	Granite	45.90798	6.77030	1025	180	5	0.983	3.00
Montsapey	MSAP12_P1_01	Polished bedrock	Schist	45.52413	6.33350	1040	0	2	0.997	9.50
	MSAP12_P1_02	Polished bedrock	Schist	45.52413	6.33350	1040	31	5	0.997	9.50
	MSAP12_P1_03	Polished bedrock	Schist	45.52413	6.33350	1040	52.5	5	0.997	9.50
	MSAP12_P1_04	Polished bedrock	Schist	45.52413	6.33350	1040	91	5	0.997	9.50
	MSAP12_P1_05	Polished bedrock	Schist	45.52413	6.33350	1040	283	5	0.997	9.50
	MSAP12_B1_06	Erratic Boulder	Granite	45.524125	6.3335	1040	0	2	0.997	9.50
Aussois	AUSS12_P1_01	Polished bedrock	Dolomite	45.22607	6.75427	1470	0	2	0.998	13.11
	AUSS12_P1_02	Polished bedrock	Dolomite	45.22607	6.75427	1470	110	5	0.998	13.11
	AUSS12_P1_03	Polished bedrock	Dolomite	45.22607	6.75427	1470	170	5	0.998	13.11
	AUSS12_P1_04	Polished bedrock	Dolomite	45.22607	6.75427	1470	250	5	0.998	13.11
	AUSS12_B1_05	Erratic Boulder 1	Micaschist	45.22607	6.75427	1470	0	2	0.994	13.11
	AUSS12_B2_06	Erratic Boulder 2	Granite	45.22607	6.75427	1470	0	2	0.994	13.11
	AUSS12_B3_07	Erratic Boulder 3	Micaschist	45.22607	6.75427	1470	0	2	0.994	13.11
	AUSS12_B3_08	Erratic Boulder 3	Micaschist	45.22607	6.75427	1470	32.5	2	0.994	10.23

© 2019 The Authors. Earth Surface Processes and Landforms published by John Wiley & Sons Ltd

Table I. (Continued)

Site name	10Be/9Be (blank corrected) (at.g^{-1})	10Be/9Be uncertainty (%)	Mass dissolved quartz (g)	Mass spike ^{9}Be (mg.g^{-1})	[^{10}Be] (10^4 at.g^{-1})	Surface exposure ages (ka) CRONUS	Internal uncertainty age (ka) CRONUS	External uncertainty age (ka) CRONUS	Depth - profile exposure ages (ka) (^{10}Be profile simulator)	Inheritance (10^4 at.g^{-1})
Les Bossons	2.860E-14	44.738	42.52	0.293	1.200 ± 0.539*	**0.83**	0.37	0.37		
	2.666E-14	16.132	37.39	0.288	1.239 ± 0.205*	**1.08**	0.18	0.16		
	5.403E-14	17.010	40.68	0.305	2.572 ± 0.440*	**3.66**	0.64	0.32		
	1.450E-14	NC	NC	NC	1.313 ± 0.598	**0.91**	0.42	0.41		
	1.160E-14	NC	NC	NC	0.829 ± 0.422	**0.58**	0.29	0.29		
Vaudagne Site 1	9.079E-14	7.927	18.79	0.306	9.597 ± 0.769**	**10.08**	0.90	0.89	**10.10 ± 1.90**	0.43 ± 0.39
	7.073E-14	21.856	13.51	0.301	10.155 ± 2.244**					
	3.648E-14	9.834	19.18	0.302	3.557 ± 0.365**					
	1.394E-14	44.738	7.52	0.303	3.056 ± 1.429**					
	0.749E-14	21.856	17.45	0.302	0.565 ± 0.146**					
	12.927E-14	7.494	11.81	0.298	21.370 ± 1.611***	**22.33**	1.89	1.88	**11.20 ± 3.90**	11.16 ± 6.49
	5.869E-14	15.509	9.67	0.296	11.457 ± 1.789***					
Vaudagne Site 2	1.478E-14	8.539	19.08	0.306	15.531 ± 1.331**	**16.41**	1.55	1.52	**15.70 ± 3.80**	1.18 ± 0.87
	8.447E-14	3.873	21.22	0.306	8.128 ± 0.513****					
	1.811E-14	8.856	21.22	0.306	1.749 ± 0.246****					
	1.050E-14	11.708	13.12	0.350	1.404 ± 0.218***					
	1.804E-14	30.175	10.01	0.304	3.128 ± 0.962***					
	1.510E-14	25.062	11.47	0.301	2.188 ± 0.569***					
	4.183E-14	9.251	6.58	0.303	12.865 ± 1.369***	**13.68**	1.55	1.52	**11.00 ± 3.10**	3.17 ± 1.89
	4.233E-14	27.866	23.43	0.300	3.401 ± 0.952***					
	4.552E-14	18.390	24.98	0.299	3.434 ± 0.636***					
Montsapey	44.500E-14	3.249	71.94	0.293	12.040 ± 0.392**	**12.82**	0.64	0.64	**12.60 ± 0.90**	0.65 ± 0.53
	10.919E-14	4.700	25.65	0.297	8.255 ± 0.393*					
	6.273E-14	9.270	20.34	0.301	5.941 ± 0.556**					
	2.409E-14	17.193	16.80	0.299	2.558 ± 0.454**					
	1.079E-14	23.602	18.05	0.302	0.915 ± 0.234**					
	14.446E-14	12.026	19.74	0.296	14.245 ± 1.716**	**15.16**	1.85	1.84		
Aussois	24.643E-14	14.611	31.09	0.298	15.616 ± 2.283*****	**11.52**	1.75	1.73	**11.70 ± 0.70**	0.43 ± 0.27
	1.431E-14	17.440	9.28	0.407	3.434 ± 0.651**					
	0.671E-14	45.589	7.43	0.307	1.130 ± 0.545**					
	0.705E-14	26.754	10.21	0.306	0.891 ± 0.274**					
	27.137E-14	4.042	28.98	0.311	19.273 ± 0.783*****	**14.31**	0.80	0.79		
	17.253E-14	6.650	16.86	0.304	20.474 ± 1.367**	**15.19**	1.10	1.09		
	39.019E-14	5.059	42.02	0.304	18.737 ± 0.949*****	**13.87**	0.88	0.88		
	16.201E-14	4.597	19.22	0.302	16.750 ± 0.788**	**12.39**	0.75	0.94		

© 2019 The Authors. Earth Surface Processes and Landforms published by John Wiley & Sons Ltd

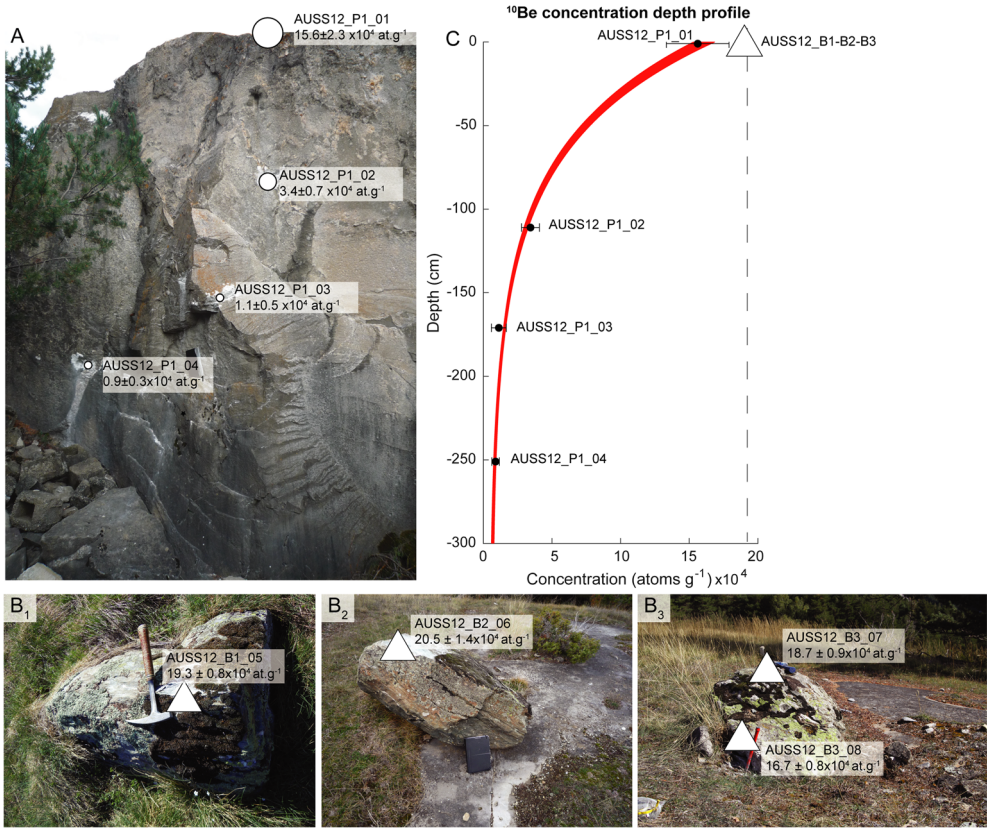

Figure 7. Aussois site: sample locations and ^{10}Be concentration in erratic boulders (AUSS12_B1, AUSS12_B2 and AUSS12_B3) and in polished surface (AUSS12_P1). (A) Vertical cross-section of the sampling polished bedrock associated with depth locations of the samples. (B) Sample locations of the three different erratic boulders (B_1, B_2, B_3). The circles and triangles illustrate the sampling positions and their sizes are dependent on the ^{10}Be concentrations of the samples. (C) Results from the Monte Carlo concentration–depth profile simulation of the polished bedrock; 2σ profile solution spaces (red line), measured ^{10}Be concentration samples with associated uncertainties (filled black circles and error bars). For comparison, we report the average surface ^{10}Be concentration (dashed line) in the three erratic boulders (white triangle). The input and output parameters of the concentration–depth profile simulation are reported in Table II. [Colour figure can be viewed at wileyonlinelibrary.com]

12.04 ± 0.39 × 10^4 atoms g^{-1} at the surface to 0.92 ± 0.23 × 10^4 atoms g^{-1} at 283 ± 2.5 cm deep (Figure 6). The calculation of the apparent exposure ages (CRONUS-Earth calculation), based only on the surface samples, yields 12.82 ± 0.64 ka and 15.16 ± 1.85 ka, for the polished bedrock and the boulder, respectively. Additionally, the Monte Carlo simulation using the depth profile samples yields a most probable exposure age of 12.60 ± 0.90 ka, with a ^{10}Be inheritance of 0.65 ± 0.53 × 10^4 atoms g^{-1} (Table II).

At Aussois, we sampled three erratic boulders, one gneiss and two micaschists, and quartz veins in the very well-preserved polished dolomitic bedrock. Each boulder was sampled on its surface and one boulder was sampled both on the surface and at the bottom. Four samples were collected from the vertical bedrock profile at 0 ± 2, 110 ± 2.5, 170 ± 2.5 and 250 ± 2.5 cm deep. The bedrock has ^{10}Be concentrations ranging from 15.61 ± 2.28 × 10^4 to 0.89 ± 0.27 × 10^4 atoms g^{-1} at 250 ± 2.5 cm deep (Figure 7 and Table I). The top surfaces of the three boulders show concentrations ranging from 20.47 ± 1.37 × 10^4 atoms g^{-1} (AUSS12_B2_06) to 18.73 ± 0.95 × 10^4 atoms g^{-1} (AUSS12_B3_07). The latter boulder has a slightly lower concentration of 16.75 ± 0.78 × 10^4 atoms g^{-1} at the bottom (AUSS12_B3_08, 32 cm from the top). Calculation of the apparent exposure ages based only on the surface samples yields 11.52 ± 1.75 ka for the polished surface and between 13.8 ± 0.88 and 15.19 ± 1.10 ka for the boulders. By considering the samples along the bedrock profile, the Monte Carlo approach simulates a most probable exposure age of 11.70 ± 0.70 ka with a ^{10}Be inheritance of 0.43 ± 0.27 × 10^4 atoms g^{-1} (Table II).

Discussion

Significance of age discrepancies

Our results indicate that the apparent exposure ages of the glacial landforms in the Western French Alpine valleys (Arc and Arve) may be significantly different from the real exposure ages. Both polished bedrock and erratic boulders are affected by this dating issue. Age discrepancies may be due to multiple causes: (1) overestimated ages determined by localized inefficient bedrock carving by the glacier (polished surfaces); (2) overestimated ages determined by significant exposure during hillslope denudation and transport of glacial sediments (erratic boulders); (3) underestimated ages caused by ancient burials by sediments or snow.

The first case is well illustrated both by the present polished bedrock of the Bossons glacier and by the older polished bedrock at Vaudagne site 2. If the abrading action of the glacier was efficient everywhere, we would have observed negligible ^{10}Be concentrations at the surface (Bossons) or at depth (Vaudagne). In contrast, at both sites we found significant ^{10}Be concentrations of the order of 10^4 atoms g^{-1} that constitute an inheritance accumulated before the last glacial retreat. The accumulation of inheritance can be explained either by a low thickness of the glacier close to the source, which was not strong enough to significantly erode the bedrock, or by the lithology of the bedrock. The lithologic parameter seems relevant for the Vaudagne bedrocks, since an inherited ^{10}Be was found in granite (site 2) but not

© 2019 The Authors. Earth Surface Processes and Landforms published by John Wiley & Sons Ltd

Table II. Left: Parameter setups used during the Monte Carlo simulations for each site (^{10}Be profile simulation 1.2; Hidy et al., 2010). Right: Modelled exposure ages and inheritance results obtained from the Monte Carlo simulations. We used the mean, maximum and minimum values mentioned in the text for the modelled exposure ages

Monte Carlo parameter setup		Results	Age (ka)	Inheritance (10^4 at.g-1)
Vaudagne Site 1 - Bedrock				
Shielding factor	0.985	mean	10.1	0.43
^{10}Be reference production rate	3.93 at.g-1.a-1	median	10.2	0.43
Site production rate	9.45 at.g-1.a-1	mode	10.5	0.41
Total muonic production	0.25 at.g-1.a-1	min chi^2	9.8	0.37
10Be inheritance range	0 - 10000 at.g-1	maximum	11.9	0.78
Chi2 cut off	5	minimum	8.1	0
		Bayesian most probable	9.9	0.4
		Bayesian 2-sigma upper	12.2	0.84
		Bayesian 2-sigma lower	8	0.06
Vaudagne Site 1 - Erratic boulder				
Monte Carlo parameter setup				
Shielding factor	0.985	mean	11.2	11.16
^{10}Be reference production rate	3.93 at.g-1.a-1	median	11.2	11.17
Site production rate	9.45 at.g-1.a-1	mode	11.2	11.03
Total muonic production	0.25 at.g-1.a-1	min chi^2	12.1	11.3
10Be inheritance range	0 - 150000 at.g-1	maximum	16	13.13
Chi2 cut off	1	minimum	8.2	8.7
		Bayesian most probable	11.2	11.3
		Bayesian 2-sigma upper	15.4	14.32
		Bayesian 2-sigma lower	6.2	7.73
Vaudagne Site 2 - Bedrock				
Shielding factor	0.985	mean	15.7	1.18
^{10}Be reference production rate	3.93 at.g-1.a-1	median	15.5	1.18
Site production rate	9.36 at.g-1.a-1	mode	14.6	1.18
Total muonic production	0.25 at.g-1.a-1	min chi^2	15.8	1.24
10Be inheritance range	0 - 35000 at.g-1	maximum	20	1.74
Chi2 cut off	5	minimum	12.3	0.65
		Bayesian most probable	14.9	1.2
		Bayesian 2-sigma upper	19.3	1.75
		Bayesian 2-sigma lower	11.8	0.51
Vaudagne Site 2 - Erratic boulder				
Shielding factor	0.985	mean	11	3.17
^{10}Be reference production rate	3.93 at.g-1.a-1	median	10.9	3.16
Site production rate	9.36 at.g-1.a-1	mode	11	3.22
Total muonic production	0.25 at.g-1.a-1	min chi^2	11.2	3.24
10Be inheritance range	0 - 50000 at.g-1	maximum	15	3.78
Chi2 cut off	1	minimum	8.9	2.56
		Bayesian most probable	10.8	3.08
		Bayesian 2-sigma upper	14.2	4.18
		Bayesian 2-sigma lower	7.4	1.74
Montsapey - Bedrock				
Shielding factor	0.993	mean	12.6	0.65
^{10}Be reference production rate	3.93 at.g-1.a-1	median	12.6	0.66
Site production rate	9.25 at.g-1.a-1	mode	12.8	0.76
Total muonic production	0.25 at.g-1.a-1	min chi^2	12.6	0.55
10Be inheritance range	0 - 15000 at.g-1	maximum	13.5	1.07
Chi2 cut off	5	minimum	11.6	0.11
		Bayesian most probable	12.7	0.75
		Bayesian 2-sigma upper	13.9	1.3
		Bayesian 2-sigma lower	11.2	0.09
Aussois - Bedrock				
Shielding factor	0.993	mean	11.7	0.43
^{10}Be reference production rate	3.93 at.g-1.a-1	median	11.7	0.43
Site production rate	13.24 at.g-1.a-1	mode	11.7	0.46
Total muonic production	0.29 at.g-1.a-1	min chi^2	11.6	0.39
10Be inheritance range	0 - 10000 at.g-1	maximum	12.3	0.54
Chi2 cut off	5	minimum	11	0.28
		Bayesian most probable	11.8	0.57
		Bayesian 2-sigma upper	15	0.96
		Bayesian 2-sigma lower	8.7	0.07

© 2019 The Authors. Earth Surface Processes and Landforms published by John Wiley & Sons Ltd

in the weaker schists (site 1). The inherited component in the granite may lead to an overestimation of the actual exposure age of ~8%.

The second case applies to the large majority of the erratic boulders studied. The boulders sampled on their tops have higher ^{10}Be concentrations than the associated polished surfaces in six of seven cases (Bossons, Vaudagne site 1, Montsapey, Aussois). At Bossons, three samples from the same boulder have three different ^{10}Be concentrations that are consistent with the heterogeneous weathering states of the boulder faces but are uncorrelated with their present positions with respect to cosmic rays. At Aussois, the three boulders have different ^{10}Be concentrations that are uncorrelated with their sizes. The boulders sampled at different depths at Vaudagne and Aussois have ^{10}Be concentration distributions that are consistent with their upside-down exposures before abandonment. In particular, if the inheritance of the erratic boulder from site 1 in Vaudagne is neglected, the real exposure age would have been overestimated by up to 80%. Multiple exposure histories have also been recognized for crystalline erratic boulders above a well-preserved moraine in the Jura Mountains (Graf et al., 2015). These results confirm that, as in fluvial contexts (Schmidt et al., 2011; Vassallo et al., 2011), the cosmogenic exposure of glacial sediments during hillslope denudation may not be negligible (Heimsath and McGlynn, 2008; Ward and Anderson, 2011). Sampling large boulders minimizes the possibility of post-depositional burial, but no relationships can be found between boulder sizes and the inherited component, as was also observed by Heyman et al. (2016). The presence of inherited ^{10}Be might be tested by core sampling through large boulders or at least by top and bottom sampling. Otherwise, a straightforward use of the ^{10}Be concentrations of erratic boulders to date glacial retreats may yield overestimated ages.

The third case (burial) is also possible but is more difficult to demonstrate. This should not be the case at Aussois, because of the exceptional high quality of preservation of its glacial and human record that strongly suggests no denudation or burying since the ice retreated. It is difficult to prove this at Montsapey, where the discrepancies in ^{10}Be concentrations between the polished bedrock and the associated erratic boulder might be derived from both burial of the bedrock and the inheritance of the boulder. We may invoke this at Vaudagne, where, regardless of the inheritance differences, the bedrock profile of site 1 has a significantly lower ^{10}Be concentration than the bedrock profile of site 2.

How to use ^{10}Be concentrations on polished bedrock and erratic boulders

Our strategy of paired sampling of polished bedrock and overlying erratic boulders highlights the pre-abandonment and post-abandonment exposure histories at given sites. The main implication of this study is that simple sampling on the tops of erratic boulders or on the surfaces of polished bedrock is often insufficient to correctly date glacial retreats. However, we are aware that finding both of these landforms at the same site is rare and that this strategy cannot be applied in most cases. Nevertheless, our results provide some recommendations, which should be necessary for future studies when using ^{10}Be concentrations, depending on the geomorphic context and on the glacial landforms.

Sampling of erratic boulders on the top and bottom sides, and possibly via cores, is crucial to estimate or at least detect inherited ^{10}Be accumulated during exhumation and transport. At one site, the age overestimation when neglecting boulder inheritance reaches ~10 000 years (approximately 80% greater than the true age). If boulders are large enough (>2 m), they are unlikely to be buried significantly by temporary sediments or snow, and exposure ages are likely to be close to the true age. Therefore, in the absence of depth profile samples, the apparent boulder ages should always be considered as the maximum post-abandonment exposure ages.

Polished bedrocks have a double ambiguity in terms of dating. On one hand, they may have an inheritance determined by inefficient local carving by the glacier. On the other hand, as they are topographically lower than boulders, they might be buried more easily by temporary sediments or by thicker snow cover. The application of depth profile sampling can be used to discriminate potential inheritance. However, without any geomorphic evidence and the ratio with another cosmogenic nuclide (e.g. ^{10}Be/^{26}Al), it is very difficult to verify the burial hypothesis. For polished bedrocks exposed over thousands of years, double ^{14}C/^{10}Be *in situ* dating can be applied to better understand the burial history (Goehring et al., 2013). Additionally, a new approach based on the coupling of OSL and ^{10}Be dating has been used to estimate the temporal and spatial variability of the post-glacial bedrock erosion rates (Lehmann et al., 2019). Therefore, when using a single TCN to date polished bedrock: (1) the inheritance should be deduced from a depth profile; (2) the calculated exposure age should be considered as the minimum post-abandonment exposure age.

Conclusions

Paired sampling of depth profiles in polished bedrock and in the overlying erratic boulder in the northwestern French Alps highlights the differences in the ^{10}Be cosmogenic exposure record for these two glacial landforms, commonly used for ice retreat dating. Therefore, the measured concentrations of these targets should be used with caution to estimate rock abandonment ages by glaciers. In our study, the ^{10}Be concentrations of erratic boulders are systematically equal to or higher than those contained in the polished surfaces. This difference may be due to pre-abandonment inheritance in the erratic boulders and/or to temporary burial of the bedrock by moraine sediments or by thicker snow cover. In the absence of complementary data, erratic boulder ages should be interpreted as maximum ages and the polished surface ages as minimum ages. Additionally, both present and past polished glacial bedrocks show that inheritance could occur in bedrock as a consequence of inefficient ice abrasion, which is unable to locally reset the ^{10}Be chronometer. The depth profiles in polished bedrocks and in erratic boulders are essential to detect and quantify ^{10}Be inheritance.

Acknowledgements—This study has received financial support from INSU-Syster programme 2012. The authors warmly thank Francis Coeur (GeoThermoChronology Platform, ISTerre) for technical support, Karim Keddadouche and Georges Aumaitres for the AMS measurements, the SAMSCIE company for drilling the cores in Vaudagne and Monstapey and Marie Thoby for her help during sampling. The authors thank the two anonymous reviewers for their helpful comments, which helped us to improve the scientific content of this work.

Data availability statement

Research data are not shared.

© 2019 The Authors. Earth Surface Processes and Landforms published by John Wiley & Sons Ltd

Conflict of interest statement

There is no conflict of interest.

References

Arnold M, Merchel S, Bourlès DL, Braucher R, Benedetti L, Finkel RC, Aumaître G, Gottdang A, Klein M. 2010. The French accelerator mass spectrometry facility ASTER: improved performance and developments. *Nuclear Instruments and Methods in Physics Research Section B: Beam Interactions with Materials and Atoms* **268**(11–12): 1954–1959. https://doi.org/10.1016/j.nimb.2010.02.107.

Balco GA, Stone JO, Lifton NA, Dunai TJ. 2008. A complete and easily accessible means of calculating surface exposure ages or erosion rates from ^{10}Be and ^{26}Al measurements. *Quaternary Geochronology* **3**(3): 174–195.

Barrett S, Starnberger R, Tjallingii R, Brauer A, Spötl C. 2017. The sedimentary history of the inner-alpine Inn Valley, Austria: extending the Baumkirchen type section further back in time with new drilling. *Journal of Quaternary Science* **32**(1): 63–79. https://doi.org/10.1002/jqs.2924.

Böhlert R, Gruber S, Egli M, Maisch M, Brandova D, Haeberli W, Ivy-Ochs S, Christl M, Kubik PW, Deline P. 2008. Comparison of exposure ages and spectral properties of rock surfaces in steep, high alpine rock walls of Aiguille du Midi, France. In *Proceedings of the 9th International Conference on Permafrost*. PAGES: Bern, Switzerland; 143–148. https://doi.org/10.5167/uzh-2822

Brown ET, Edmond JM, Raisbeck GM, Yiou F, Kurz MD, Brook EJ. 1991. Examination of surface exposure ages of Antarctic moraines using in situ produced ^{10}Be and ^{26}Al. *Geochimica et Cosmochimica Acta* **55** (8): 2269–2283.

Chenet M, Brunstein D, Jomelli V, Roussel E, Rinterknecht V, Mokadem F, Biette M, Robert V, Léanni L. 2016. ^{10}Be cosmic-ray exposure dating of moraines and rock avalanches in the Upper Romanche valley (French Alps): evidence of two glacial advances during the Late Glacial/Holocene transition. *Quaternary Science Reviews* **148**: 209–221. https://doi.org/10.1016/j.quascirev.2016.07.025.

Coutterand S, Nicoud G. 2005. Les stades de retrait du glacier de l'Arve entre le verrou de cluses et l'ombilic de chamonix au cours du tardiglaciaire (Vallée de l'Arve, Haute-Savoie). *Quaternaire* **16**(2): 85–94. https://doi.org/10.4000/quaternaire.296.

Delmas M. 2009. Chronologie et impact géomorphologique des glaciations quaternaires dans l'est des Pyrénées. PhD thesis. Laboratoire de Recherche En Géographie Physique MEDI-TERRA, Université de Perpignan, LGP Meudon, Université de Paris 1 Panthéon Sorbonne. Available: http://tel.archives-ouvertes.fr/tel-00519194/

Delmas M, Calvet M, Gunnell Y, Braucher R, Bourlès D. 2011. Palaeogeography and ^{10}Be exposure-age chronology of Middle and Late Pleistocene glacier systems in the northern Pyrenees: implications for reconstructing regional palaeoclimates. *Palaeogeography, Palaeoclimatology, Palaeoecology* **305**(1): 109–122.

Delmas M, Gunnell Y, Braucher R, Calvet M, Bourlès D. 2008. Exposure age chronology of the last glaciation in the eastern Pyrenees. *Quaternary Research* **69**(2): 231–241.

Dunne J, Elmore D, Muzikar P. 1999. Scaling factors for the rates of production of cosmogenic nuclides for geometric shielding and attenuation at depth on sloped surfaces. *Geomorphology* **27**(1–2): 3–11. https://doi.org/10.1016/S0169-555X(98)00086-5.

Fabel D, Stroeven AP, Harbor J, Kleman J, Elmore D, Fink D. 2002. Landscape preservation under Fennoscandian ice sheets determined from in situ produced ^{10}Be and ^{26}Al. *Earth and Planetary Science Letters* **201**(2): 397–406. https://doi.org/10.1016/S0012-821X(02)00714-8.

Fourneaux JC. 1976. Les formations quaternaires de la vallée de l'Isère dans l'ombilic de Grenoble. *Geologie Alpine* **52**: 31–72.

Ganti V, Von Hagke C, Scherler D, Lamb MP, Fischer WW, Avouac J-P. 2016. Supplementary materials for time scale bias in erosion rates of glaciated landscapes. *Science Advances*: 2. e1600204. https://doi.org/10.1126/sciadv.1600204.

Godon C, Mugnier JL, Fallourd R, Paquette JL, Pohl A, Buoncristiani JF. 2013. The Bossons glacier protects Europe's summit from erosion. *Earth and Planetary Science Letters* **375**: 135–147. https://doi.org/10.1016/j.epsl.2013.05.018.

Goehring BM, Muzikar P, Lifton NA. 2013. An in situ ^{14}C–^{10}Be Bayesian isochron approach for interpreting complex glacial histories. *Quaternary Geochronology* **15**: 61–66. https://doi.org/10.1016/j.quageo.2012.11.007.

Graf A, Akçar N, Ivy-Ochs S, Strasky S, Kubik PW, Christl M, Burkhard M, Wieler R, Schlüchter C. 2015. Multiple advances of Alpine glaciers into the Jura Mountains in the Northwestern Switzerland. *Swiss Journal of Geosciences* **108**: 225–238. https://doi.org/10.1007/s00015-015-0195-y.

Guillon H, Mugnier J-L, Buoncristiani J-F, Carcaillet J, Godon C, Prud'homme C, Vander Beek P, Vassallo R. 2015. Improved discrimination of subglacial and periglacial erosion using ^{10}Be concentration measurements in subglacial and supraglacial sediment load of the Bossons glacier (Mont Blanc massif, France). *Earth Surface Processes and Landforms* **40**(9): 1202–1215. https://doi.org/10.1002/esp.3713.

Heimsath AM, McGlynn R. 2008. Quantifying periglacial erosion in the Nepal high Himalaya. *Geomorphology* **97**(1–2): 5–23. https://doi.org/10.1016/j.geomorph.2007.02.046.

Herman F, Beyssac O, Brughelli M, Lane SN, Leprince S, Adatte T, Lin JYY, Avouac JP, Cox SC. 2015. Erosion by an Alpine glacier. *Science* **30**(6257): 193–195. https://doi.org/10.1126/science.aab2386.

Heyman J, Applegate PJ, Blomdin R, Gribenski N, Harbor JM, Stroeven AP. 2016. Boulder height: exposure age relationships from a global glacial ^{10}Be compilation. *Quaternary Geochronology* **34**: 1–11. https://doi.org/10.1016/j.quageo.2016.03.002.

Hidy AJ, Gosse JC, Pederson JL, Mattern JP, Finkel RC. 2010. A geologically constrained Monte Carlo approach to modeling exposure ages from profiles of cosmogenic nuclides: an example from Lees Ferry, Arizona. *Geochemistry, Geophysics, Geosystems* **11**(9): Q0AA10. https://doi.org/10.1029/2010GC003084.

King GE, Robinson RAJ, Finch AA. 2014. Towards successful OSL sampling strategies in glacial environments: deciphering the influence of depositional processes on bleaching of modern glacial sediments from Jostedalen, southern Norway. *Quaternary Science Reviews* **89**: 94–107. https://doi.org/10.1016/j.quascirev.2014.02.001.

Lal D. 1991. Cosmic ray labeling of erosion surfaces in situ nuclide production rates and erosion models. *Earth and Planetary Science Letters* **104**(2): 424–439.

Lehmann B, Herman F, Valla PG, King GE, Biswas RH. 2019. Evaluating post-glacial bedrock erosion and surface exposure duration by coupling in situ optically stimulated luminescence and ^{10}Be dating. *Earth Surface Dynamics Discussions* **7**: 633–662. https://doi.org/10.5194/esurf-2018-97.

Menzies, J. (2018). Glacial Geomorphology. Reference Module in Earth Systems and Environmental Sciences. Update of H. French and J. Harbor, 8.1 The Development and History of Glacial and Periglacial Geomorphology, In *Treatise on Geomorphology*, Shroder JF (ed). Academic Press: San Diego, **2013**.

Merchel S, Herpers U. 1999. An update on radiochemical separation techniques for the determination of long-lived radionuclides via accelerator mass spectrometry. *Radiochimica Acta* **84**(4): 215–220. https://doi.org/10.1524/ract.1999.84.4.215.

Nehl G. 1981. Les gravures rupestres de Haute Maurienne. *Travaux Scientifiques Du Parc National de La Vanoise* **X**: 9–35 **XI**: 9–27.

Nicoud G, Royer G, Corbin J, Lemeille F, Paillet A. 2002. Creusement et remplissage de la vallée de l'Isère au Quaternaire récent: apports nouveaux du forage GMB1 (1999) dans la région de Grenoble (France). *Géologie de la France* **4**(1999): 39–49.

Nishiizumi K, Imamura M, Caffee MW, Southon JR, Finkel RC, McAninch J. 2007. Absolute calibration of ^{10}Be AMS standards. *Nuclear Instruments and Methods in Physics Research Section B: Beam Interactions with Materials and Atoms* **258**(2): 403–413. https://doi.org/10.1016/j.nimb.2007.01.297.

Protin M, Schimmelpfennig I, Mugnier JL, Ravanel L, Le Roy M, Deline P, Favier V, Buoncristiani JF, Aumaître G, Bourlès DL, Keddadouche K. 2019. Climatic reconstruction for the Younger Dryas/Early Holocene transition and the Little Ice Age based on paleo-extents of Argentière glacier (French Alps). *Quaternary Science Reviews* **221**:105863. https://doi.org/10.1016/j.quascirev.2019.105863.

© 2019 The Authors. Earth Surface Processes and Landforms published by John Wiley & Sons Ltd

Schmidt S, Hetzel R, Kuhlmann J, Mingorance F, Ramos VA. 2011. A note of caution on the use of boulders for exposure dating of depositional surfaces. *Earth and Planetary Science Letters* **302**(1–2): 60–70. https://doi.org/10.1016/j.epsl.2010.11.039.

Stone JO. 2000. Air pressure and cosmogenic isotope production. *Journal of Geophysical Research* **105**(B10): 23753–23759.

Thirault E. 2008. Enjeux et perspectives du Néolithique alpin: l'exemple de la Maurienne (Savoie – France). *Palethnologie* **1**: 410–426.

Vassallo R, Ritz JF, Carretier S. 2011. Control of geomorphic processes on ^{10}Be concentrations in individual clasts: complexity of the exposure history in Gobi-Altay range (Mongolia). *Geomorphology* **135**(1–2): 35–47. https://doi.org/10.1016/j.geomorph.2011.07.023.

Ward DJ, Anderson RS. 2011. The use of ablation-dominated medial moraines as samplers for ^{10}Be-derived erosion rates of glacier valley walls, Kichatna Mountains, AK. *Earth Surface Processes and Landforms* **36**(4): 495–512. https://doi.org/10.1002/esp.2068.

Young NE, Schaefer JM, Briner JP, Goehring BM. 2013. A ^{10}Be production-rate calibration for the Arctic. *Journal of Quaternary Science* **28**(5): 515–526. https://doi.org/10.1002/jqs.2642.

© 2019 The Authors. Earth Surface Processes and Landforms published by John Wiley & Sons Ltd